Permeability Determination from On-the-Fly Piezocone Sounding

Derek Elsworth[1] and Dae Sung Lee[2]

Abstract: Solutions are developed for the steady, partially drained, fluid pressure field that develops around a moving penetrometer. These include rigorous solution for a point volumetric dislocation moving in a saturated elastic soil and an approximate solution for a pseudostatic, finite-volume, penetrometer moving in a nondilatant soil. These solutions provide a consistent framework for viewing the penetration process, and enable the nondimensional sounding indices of normalized tip resistance Q_t, friction factor F_r, and pore pressure ratio B_q, to be straightforwardly linked to important material properties of the soil, most notably that of permeability, via a nondimensional permeability K_D. This factor K_D is inversely proportional to penetration rate, and is directly proportional to both permeability and vertical in situ effective stress. Simple relationships are developed to link these nondimensional sounding metrics, via K_D. Most notably, the resulting simple relationship $K_D = 1/B_q Q_t$ enables soil permeability to be determined from peak fluid pressures recorded on-the-fly. Importantly, these parameterizations enable plots of $B_q - Q_t$, $F_r - Q_t$, and $B_q - F_r$ to be contoured for K_D, and hence for permeability. These plots define the relative superiority of using $B_q - Q_t$ data pairs over those for $F_r - Q_t$ and $B_q - F_r$, in defining permeability. Similarly, the feasible range of permeabilities that may be recovered from peak pressure data are defined; permeabilities must be sufficiently high that penetration is not undrained, and sufficiently low that the resulting pressure response is not null (fully drained). These limits are a natural product of the analysis and represent permeabilities in the range $10^{-4} - 10^{-7}$ m/s. The utility of these characterizations is confirmed with data from two locations where cone soundings are correlated with independently estimated permeabilities.

CE Database subject headings: Soil permeability; Penetrometers; Saturated soils.

Introduction

Piezocone sounding is a rapid, minimally invasive and inexpensive method for determining the mechanical and transport properties of soil types, their distribution in space, and the type and distribution of the soil saturants (e.g., Campanella and Robertson 1988; Mitchell and Brandon 1998). In determining soil transport properties, the absolute magnitude or rate of decay of penetration-generated excess pore fluid pressures are recorded, and correlated with the coefficients of consolidation c_v or permeability K, of the soil (the term "permeability" is used as a contraction for "coefficient of permeability," throughout the following). Data reduction techniques may be divided broadly between methods that employ empirical correlations, and those that measure the generation or dissipation of pore fluid pressures, at the cone tip or sleeve, either concurrent with penetration or post-arrest. The latter include pump-type fluid injection tests.

[1]Professor, Dept. of Energy and Geo-Environmental Engineering, Pennsylvania State Univ., University Park, PA 16802-5000 (corresponding author). E-mail: elsworth@psu.edu

[2]PhD Candidate, Dept. of Energy and Geoenvironmental Engineering, Pennsylvania State Univ., University Park, PA 16802-5000.

Empirical Methods

The empirical methods involve matching soil classification derived from cone sounding data with anticipated magnitudes of permeability coefficient. The corrected magnitudes of tip resistance q_t, pore pressure ratio B_q and sleeve friction f_s (Douglas and Olsen 1981; Robertson et al. 1986) are used to classify soils while the soil type or estimated grain size are used to estimate permeability coefficient. These concepts have been extended to match both pore pressure ratios (Manassero 1994) and sleeve friction magnitudes (Olsen 1994) with independently measured coefficients of permeability. Alternative methods involve estimating coefficient of permeability directly from end bearing (Smythe et al. 1989; Chiang et al. 1992) when sleeve friction is known. Although useful, the data supporting these correlations are meager, and they are correspondingly not rigorously validated.

Pore Pressure Response Methods

Permeabilities may also be evaluated from coefficient of consolidation through the standard correlation with an independently evaluated coefficient of volume compressibility m_v, as $K = \gamma_w m_v c_v$, where γ_w is the unit weight of water. Coefficients of consolidation may be evaluated by recording the rate of decay of cone-generated pore pressures following the arrest of penetration. Several methods are used to calculate c_v (e.g., House et al. 2001). All require that a prearrest pore pressure distribution may be determined. Most assume undrained loading for this evaluation, and incorporate cavity expansion (Torstensson 1977; Burns and Mayne 1998) or strain path models (Baligh 1985; Baligh and Levadoux 1986; Levadoux and Baligh 1986; Teh and Houlsby 1991; Danziger et al. 1997) to define initial pore pressure

JOURNAL OF GEOTECHNICAL AND GEOENVIRONMENTAL ENGINEERING © ASCE / MAY 2005 / **643**

J. Geotech. Geoenviron. Eng., 2005, 131(5): 643-653

distributions that may subsequently dissipate to background. These evaluations compare well with field (Baligh and Levadoux 1986; Levadoux and Baligh 1986) and calibration chamber (Kurup et al. 1994) results. Predictions from complex (Baligh and Levadoux 1986) and simple material models (Teh and Houlsby 1991) compare well with more rigorous representations of finite strain continuum behavior for clays (Kiousis and Voyiadjis 1985; Voyiadjis and Abu-Farsakh 1997; Voyiadjis and Song 2000), sands (Cividini and Gioda 1988), and clays to sands (van den Berg 1994). For linear soil behavior, a variant of these methods may be applied to account for partial drainage in an effective stress analysis (Elsworth 1991, 1993, 1998) and yields similar results to those from strain path and continuum models.

Estimates of coefficients of consolidation result directly from these analyses. Transformation to permeabilities requires that volume compressibility is independently evaluated. As this value is generally not known a priori, volume compressibility is estimated from one of many empirical equations, yielding permeability that is subject to great uncertainty (Lunne et al. 1997). Other direct correlations of coefficient of consolidation with coefficient of permeability exist (Schmertmann 1978) but are not broadly confirmed either by data (Robertson et al. 1992), or on functional grounds.

Permeability values can also be determined using pseudopenetrometers, such as drive-point piezometers, the poly vinyl chloride miniwell (Auxt and Wright 1995), the BAT permeameter (Chiang et al. 1992), or the Hydrocone (Scaturo and Widdowson 1997). These devices are used to conduct slug or pump tests following penetration arrest or installation. Modified piezometer/penetrometers have also been developed for saturated soils (Konrad and Frechette 1995) and to determine water (Gribb et al. 1998) and gas (Lowry 1998) permeabilities in unsaturated soils. These methods all work well, but require that penetration is arrested.

On-the-fly Evaluations

On-the-fly evaluations (Elsworth 1993) do not require penetrometer arrest, and the subsequent monitoring of pressure dissipation. Rather, permeabilities are evaluated from the magnitudes of peak pore pressures recorded at the penetrometer tip. When pore pressures are generated around the cone tip and dissipate concurrently (as in sands), the behavior may be viewed as a controlled strain-rate test, where rate of dissipation is controlled by permeability. Low permeabilities impede drainage, resulting in higher pore pressures and dissipation rates controlled by the permeability. This behavior was originally modeled using simple linear poroelastic models representing concurrent generation and dissipation of pore pressures around a moving blunt penetrometer (Elsworth 1990, 1991, 1992, 1993), but may also be evaluated using models representing the tapered form (Elsworth 1998) of the tip and more realistic constitutive parameters (Song et al. 1999; Voyiadjis and Song 2000). Regardless of the method used, functional relations result that link permeability K, with penetration rate U, and reciprocal excess pore pressure at the tip p, relative to the static pore pressure magnitude p_s, as $K \propto U/(p-p_s)$. This result shows that permeability values can be determined, at least in principle, from pore pressure magnitudes recorded at single or multiple sensor locations, "on-the-fly." Appropriate analyses are developed in the following that support this functional relation, and are compared with results from partially drained penetration in sands. For the first time, analytical correlations are developed that link magnitudes of on-the-fly pore

pressure measurements with end-bearing and friction-factor indices, as a method to evaluate in situ permeabilities. These are developed as an adjunct to available empirical correlations.

Steady Pore Pressures Generated around Moving Penetrometer

Relations may be developed to represent the steady pore fluid pressures that develop around a penetrometer under steady penetration at penetration rate U. These models necessarily employ simple linearized constitutive relations, but incorporate the important influence of a porous medium migrating past the penetrometer tip, albeit in a simplified form. Dislocation models (Elsworth 1991, 1993) may be applied to represent a penetrometer of infinitesimal radius, but suffer the disadvantage that penetration-induced pressures become singular at the assumed penetrometer tip. The approximate solution for a finite radius penetrometer avoids this shortcoming, as explored in the following sections.

Infinitesimal-Radius Penetrometer

Dislocation models allow undrained to drained conditions to be represented during penetration and following arrest for blunt and tapered penetrometers (Elsworth 1991, 1998). The same parameters are used to represent undrained and partially drained behavior, including estimation of cavity expansion stresses that represent tip resistance, q_t (Elsworth 1993). Pore pressures generated behind and ahead of the tip are defined by representing the penetrometer as a series of volumetric dislocations, arranged along the trajectory of the penetrometer, and activated sequentially as the tip advances (Elsworth 1993). As this linear distribution is successively "inflated," and retained in this inflated state, pore pressures that are induced around the tip and shaft may be straightforwardly determined as (Elsworth 1991)

$$p - p_s = \frac{U a \gamma_w}{4K} \frac{a}{x} \exp - \frac{U(\sqrt{x^2 - x})}{c_v} \tag{1}$$

where c_v=coefficient of consolidation; a=radius of the penetrometer; and x=location where the excess pore pressure $p-p_s$ is measured, relative to the most recently activated dislocation, that concurrently represents the penetrometer tip (x is always positive on the shaft, behind the tip). Importantly, along the penetrometer shaft, the steady pore pressures decay with the reciprocal of length from the tip, and are defined as

$$\frac{4K(p - p_s)}{U \gamma_w a} = \frac{a}{x}$$

(since for positive x, $\sqrt{x^2 - x} = 0$), enabling permeability to be, in principle, recovered from the steady pressure distribution at the tip and along the shaft. The main problem in applying this method is that the soil is assumed linearly elastic, and induced pressures are singular at the penetrometer tip. Hence, an alternative representation is sought.

Finite-Radius Penetrometer

Similar to the point moving dislocation, approximate solutions may be developed for the fluid pressure field that develops around a migrating dislocation of finite size. The approach is similar to that for a point dislocation and considers penetration as analogous to injecting a fluid volume equivalent to that introduced, per unit
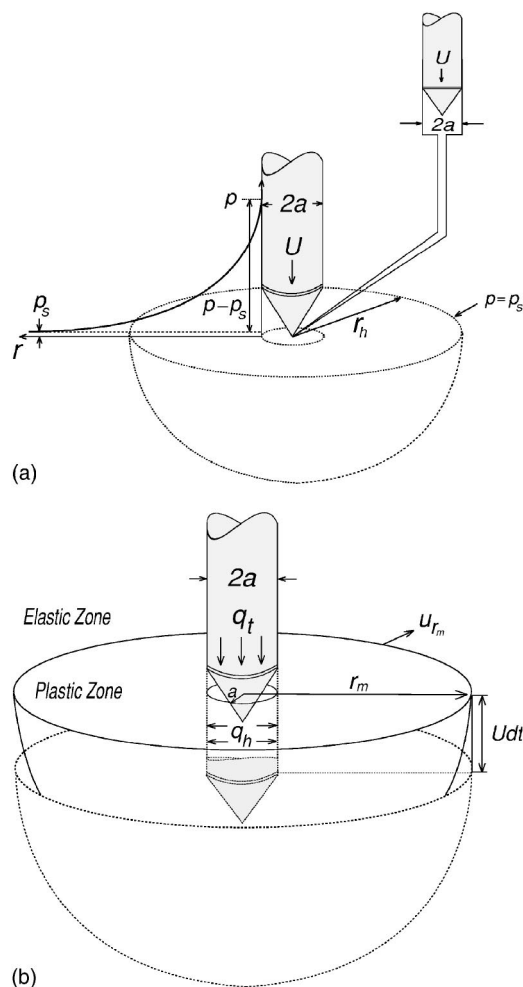
Fig. 1. Geometry of process zone surrounding advancing penetrometer: (a) hydraulic behavior defined with pressure p, induced at tip, and remote pressure p_s, at radius r_h. (b) Mechanical behavior defined by mechanical process zone of radius, r_m, with displacement $u_{\rm rm}$ at elastic–plastic boundary, and with tip stress of magnitude q_t

time, by the insertion of the penetrometer column (Fig. 1), of diameter $2a$, and distributed over the spherical contour representing the penetrometer tip, that moves at a penetration rate (or synonymous insertion velocity), U. This fluid volume, equivalent to $dV = \pi a^2 U$, per unit time, is injected into a static location, and the resulting difference between this and the point dislocation analysis is that the dynamic flow system is assumed as illustrated in Fig. 1(a), and as Fig. 1(b) for the mechanical system. The principal requirement is for the system to be in a dynamic steady state, and the contour of injection is now of finite radius, not infinitesimal. The resulting approximate solution to this spherically symmetric geometry is obtained by applying continuity and Darcy's law to yield

$$p - p_s = \frac{\gamma_w}{4\pi Ka}\left(1 - \frac{a}{r_h}\right)dV = \frac{Ua\gamma_w}{4K}\left(1 - \frac{a}{r_h}\right) \qquad (2)$$

where p_s=static pore fluid pressure at radius r_h from the penetrometer, relative to the pressure measured at the penetrometer face p. This simply represents the solution where fluid flux is injected at the interior surface of the spherical shell [Fig. 1(a)] at a rate equivalent to the insertion volume, per unit time, of the penetrometer. If r_h corresponds to the mechanical process zone,
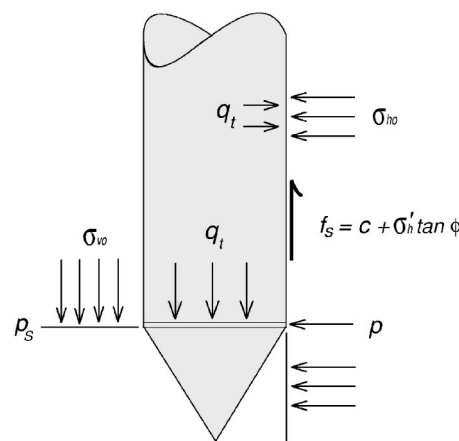

Fig. 2. Tip local conditions. Cone expansion stress is q_t.

then sensible magnitudes of a/r_h are in the range $1/10 < a/r_h < 1/2$, and the bracketed term of Eq. (2) varies between unity and on-half. Alternately, if changes in permeability in the process zone are minimal, then the hydraulic boundary is set at $r_h \to \infty$, and correspondingly, $(1 - a/r_h) \to 1$ with no loss of generality, to yield

$$p - p_s = \frac{Ur_wa}{4K}\left(1 - \frac{a}{r_h}\right) = \frac{U\gamma_w a}{4K} \qquad (3)$$

Notably, this solution is similar to that recovered for a moving point dislocation [Eq. (1)], but importantly includes the crucial effect of a finite size penetrometer tip. Despite this consideration, this simplified solution is unable to discriminate between pore pressures measured on the tip, shoulder, or shaft, as all are represented on the idealized geometry of the spherical inclusion surface.

Piezocone Indices

A variety of normalized indices are available to define the end-bearing, frictional, and pore pressure response recorded around the tip of an advancing piezocone. The interrelations of these parameters are illustrated in Fig. 2. The dimensionless magnitudes of tip resistance Q_t, and sleeve friction F_r, may be defined as

$$Q_t = \frac{q_t - \sigma_{v0}}{\sigma'_{v0}}$$

$$F_r = \frac{f_s}{q_t - \sigma_{v0}} \qquad (4)$$

where q_t=corrected tip resistance; f_s=magnitude of sleeve friction, defined in units of stress; σ_{v0}=initial magnitude of in situ vertical stress; and the prime denotes effective stress. In addition to these mechanical parameters, pore pressure ratio, B_q is defined as

$$B_q = \frac{p - p_s}{q_t - \sigma_{v0}} = \frac{p - p_s}{\sigma'_{v0}}\frac{1}{Q_t} \qquad (5)$$

where the second part of Eq. (5) results from the substitution of Eq. (4). Notably, Eq. (5) links B_q and Q_t. Normalized sleeve friction, F_r, may be related to pore pressure, by noting that $f_s = c + \sigma'_h \tan \phi$ or $f_s = c + (\sigma_h - p)\tan \phi$ where (c, ϕ) are the soil strength

parameters and σ'_h is the horizontal effective stress defined in Fig. 2. The insertion of the probe changes the horizontal stress. We assume that the total horizontal stress, σ_h, is equal to spherical cavity expansion stress, q_t, applied at the cone tip as $\sigma_h = q_t$. Where end bearing is idealized as spherical expansion, symmetry requires that the radial stress is uniform in all directions within the tip-local process zone. Hence, where the friction sleeve is sufficiently close to the cone tip to be significantly contained within the process zone, the equating of end bearing and horizontal stresses will be a reasonable approximation. Thus, $f_s = c + (q_t - p)\tan\phi$, which following rearrangement and substitution of Eqs. (4) and (5) yields

$$F_r = c_R + \left[1 + \frac{1}{Q_t} - B_q\right]\tan\phi \qquad (6)$$

with $c_R = c/(q_t - \sigma_{v0})$ where it is implicitly assumed that the coefficient of friction at the sleeve–soil interface is $\tan\phi$. This enables the dimensionless sleeve friction to be determined from fundamental material characteristics. With these quantities determined, an evaluation of the permeability of the penetrated soil may be defined.

Infinitesimal-Radius Penetrometer

With magnitudes of penetration induced pore pressure, $p - p_s$, available in Eq. (1), substituting this relation directly into Eq. (5) enables plots of Q_t versus B_q to be contoured for permeability, for the case of an infinitesimal radius penetrometer. The resulting relationship is

$$B_q = \frac{1}{\sigma'_{v0}}\frac{1}{Q_t}\frac{Ua\gamma_w}{4K}\frac{a}{x}\exp-\frac{U(\sqrt{x^2}-x)}{c_v} = \frac{1}{K_D Q_t}\frac{a}{x}\exp-\frac{U(\sqrt{x^2}-x)}{c_v} \qquad (7)$$

where $K_D = (4K\sigma'_{v0})/(Ua\gamma_w)$ and $=$ nondimensional index, directly proportional to coefficient of permeability K. Where measurements of pressure are taken on the shaft, only, Eq. (7) reduces to a simpler form as x is constrained to be positive, behind the tip. In this instance, the role of the nondimensional penetration rate $U_D = Ua/2c_v$ (Elsworth 1991) is eliminated in controlling the form of the shaft pressure distribution during steady penetration, where it varies as $(p - p_s) \propto 1/x$. The magnitude of peak pressure is modulated by a different nondimensional parameter K_D as Eq. (7) becomes

$$B_q = \frac{1}{K_D Q_t}\frac{a}{x} \qquad (8)$$

where the factor x/a is defined by the location of the pore pressure transducer, and is sensibly on the order of 1 at the tip ($x = a$), and equal to the normalized separation behind the tip for shaft-mounted transducers. Plots of $B_q - Q_t$ are shown in Fig. 3 for tip pressures ($a/x = 1$), contoured for values of K_D, and permeability, where σ'_{v0} is taken as 100 kPa. This figure notes the variation of K_D, which is directly proportional to permeability K, enabling permeability to be determined, at least in theory. The magnitude of in situ effective stress is the sole remaining parameter and this may be straightforwardly evaluated.

This figure is useful, but suffers two shortcomings. The first is that no failure around the penetrometer is accommodated, with the result that the potential influence of dilation or contraction is not incorporated. Second, where pore fluid pressures are recorded
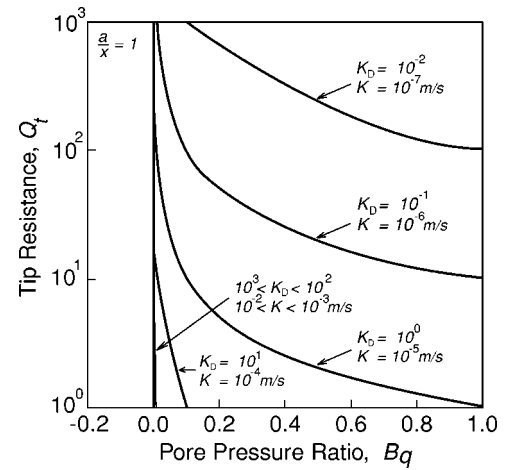

Fig. 3. Contoured plot of $B_q - Q_t$ contoured for K_D for penetrometer of infinitesimal radius with $x/a = 1$. Conversion between K_D and K is performed for effective stresses at 10 m depth, for penetration of a standard cone at 2 cm/s

at the tip, Eq. (8) is singular and no determination of permeability is possible. For this reason, recourse is made to the solution for a finite radius penetrometer.

Finite-Radius Penetrometer

The problem of singular pressures at the tip of a moving dislocation is circumvented if the approximate solution for steady pressure distribution around a migrating cavity [defined in Eq. (3)] is used. Substituting Eq. (3) into Eq. (5) enables the pore pressure ratio B_q to be defined as

$$B_q \approx \frac{Ua\gamma_w}{4K}\frac{1}{(q_t - \sigma_{v0})} = \frac{Ua\gamma_w}{4K\sigma'_{v0}}\frac{1}{Q_t} = \frac{1}{K_D Q_t} \qquad (9)$$

This defines a relation between $B_q - Q_t$ that is plotted in Fig. 4(a) for a variety of magnitudes of the nondimensional parameter K_D, directly proportional to permeability. This is identical to Fig. 3 (for $x/a = 1$), but is representative of a finite-radius penetrometer tip.

Where strains within the tip-process zone are sufficiently large to destroy the initial cohesion, $c \rightarrow 0$ and hence $c_R \rightarrow 0$ in Eq. (6). Eq. (6) links the three cone metrics, B_q, Q_t, and F_r via the frictional strength of the soil. Noting from Eq. (9) that $Bq = 1/K_D Q_t$ enables Eq. (6) to be rewritten solely in terms of $Q_t - F_r$ as

$$K_D^{Q_t - F_r} = \frac{1}{Q_t\left[1 + \dfrac{1}{Q_t} - \dfrac{F_r}{\tan\phi}\right]} \qquad (10)$$

enabling K_D to be determined from Q_t and F_r, for an assumed frictional strength, ϕ. Similarly, substituting $1/Q_t = B_q K_D$ into Eq. (6) yields

$$K_D^{B_q - F_r} = \frac{1}{B_q}\left[\frac{F_r}{\tan\phi} - 1 + B_q\right] \qquad (11)$$

Correspondingly, Eqs. (9), (10), and (11) provide estimates of permeability K_D, derived from the three potential pairs of cone penetration test (CPT) metrics, namely, $B_q - Q_t$, $F_r - Q_t$ and $B_q - F_r$. Notably, these require an assumed frictional strength, ϕ, but yield two independent evaluations of permeability K_D, as shown in Fig. 4. It should be noted that these results are derived from
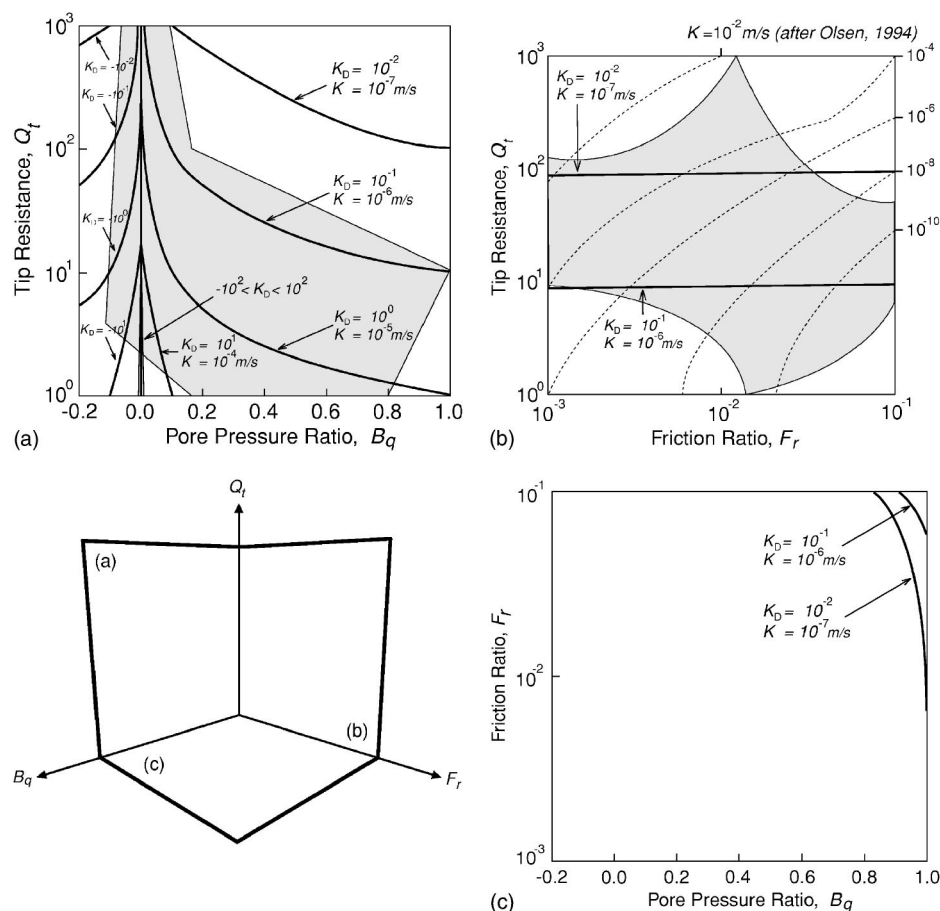
Fig. 4. Contoured plots of: (a) B_q–Q_t; (b) F_r–Q_t; and (c) B_q–F_r contoured for K_D for penetrometer of finite radius. Values of K are shown for standard cone with $\sigma'_{v0} = 100$ kPa, and $U = 2$ cm/s. Frictional strength $\phi = 30°$ is assumed for (b) and (c). The empirical results of Olsen (1994) are shown dashed in (b), and solid ranges of Robertson (1990) are shown shaded in (a) and (b).

only two independent assumptions—those embodied in the flow behavior [Eq. (3)] and the assumed sleeve friction [Eq. (6)]. Since the flow relation [Eq. (3)] is substituted into the sleeve friction relation [Eq. (6)], the plots for K_D with respect to F_r–Q_t and B_q–F_r depend principally on $K_D = 1/B_q Q_t$ and frictional strength, ϕ.

This results in Figs. 4 and 5, with the individual graphs, (a) through (c), nominally representing a projection on the side-walls and single base of the box defined by the axes B_q–Q_t–F_r. However each of relations (9), (10), and (11) are defined by only two of these parameters, and therefore do not represent the walls or base of this box, per se. The resulting relations are shown for $\phi = 30°$ in Fig. 4, and for $\phi = 10°$ in Fig. 5, showing no influence on the relations for B_q–Q_t and only slight influence for the other two relations [Figs. 4(b and c) and 5(b and c)].

The graphs of Fig. 4 indicate that permeability may be determined from judicious choice of cone metrics, B_q, Q_t, and F_r, although some of these parameters are likely more useful than others. In all instances, permeability is determined by the surrogate parameter K_D, requiring knowledge of effective stress σ'_{v0}. Plots of B_q–Q_t [Figs. 4(a) and 5(a)] give the broadest spread of K_D values, and appear most useful, defining a range of about 3–4 orders of magnitude where permeabilities may be determined. Outside this range, either the steady assumption is violated (low K_D representing low permeability), or induced pressures are too low to be detected (high K_D or very high permeability).

The F_r–Q_t curves [friction factor versus tip resistance; Figs.

4(b) and 5(b)] indicate that these parameters are potentially poor discriminants of permeability, as might be expected—the role of pore pressures are only incorporated indirectly in the parameters F_r and Q_t, rather than overtly as in B_q. This is seen as a fundamental drawback of not using B_q in the evaluation of permeability. Notably, these curves do not parallel the empirical results of Olsen (1994), where permeability is defined based on heuristic classification of soil gradation, with Olsen's (1994) contours illustrated on the plot of Figs. 4(b) and 5(b), together with the parameter ranges of Robertson (1990).

For completeness, the curves of B_q–F_r (pore pressure ratio versus friction factor) are also shown, as illustrated in Figs. 4(c) and 5(c). These curves encompass a broad range of K_D values, and may be potentially useful in determining permeability magnitudes, as examined later.

Available Data

Field data correlating cone sounding data with field-measured permeabilities are meager, and carefully controlled soundings and finely resolved material property data are necessary to confirm the utility of the models, proposed earlier. However, to investigate the veracity of the proposed models, two approaches are possible. The first involves the correlation against data recovered from carefully executed tests, with correlated measurements of permeability. The second involves attempting to determine magnitudes
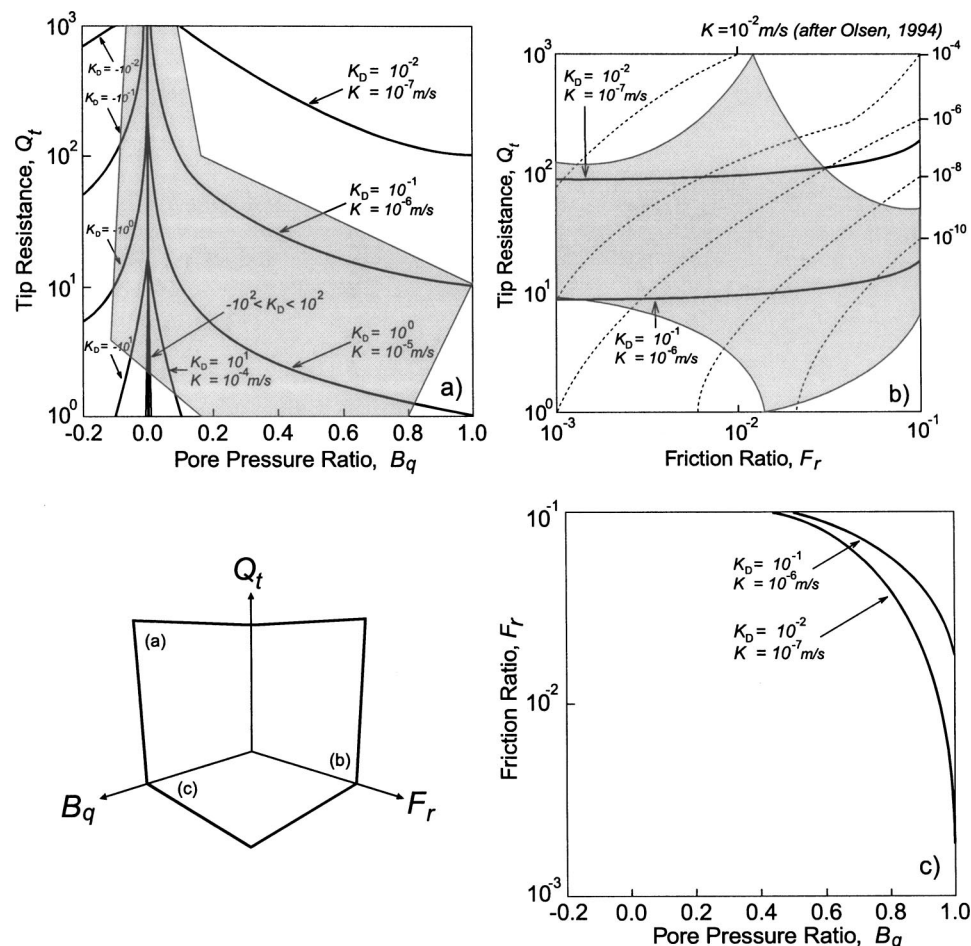
Fig. 5. Contoured plots of: (a) B_q–Q_t, (b) F_r–Q_t, and (c) B_q–F_r contoured for K_D for penetrometer of finite radius. Values of K are shown for standard cone with $\sigma'_{v0}=100$ kPa, and $U=2$ cm/s. Frictional strength $\phi=10°$ is assumed for (b) and (c). Empirical results of Olsen (1994) are shown dashed in (b), and solid ranges of Robertson (1990) are shown shaded in (a) and (b).

of K_D, by sequentially using alternate pairs of the penetrometer indices (B_q, F_r, and Q_t) to determine which twin pairs give consistent predictions of K_D. Both approaches are documented in the following.

The data used here are for normally consolidated alluvial sands and silts (Kegley 1993; Thibault 1996) at the Savannah River Site in Georgia and for hydraulically deposited silty sands at Treasure Island, Calif. (Richard and Alba 2000). In each instance, the penetration is "partially drained" making this analysis appropriate, and correlating permeability data are available from either laboratory tests on recovered samples, or from permeability estimates recovered from grain-size distributions (Robertson 1990, Hryciw et al. 2003). The use of estimates based on grain size distributions is necessitated by the paucity of field measured permeabilities in sands.

Correlation with Field Data

Piezocone data are used from two sites, specifically where confirmatory measurements of permeability may be defined. In each case, the full suite of three parameters B_q–F_r–Q_t is available and these data are used in a triplet of pairs, B_q–Q_t, F_r–Q_t, and B_q–F_r, to evaluate K_D. With K_D determined, magnitudes of permeability are recovered.

Savannah River Site

A series of soundings are available from the Savannah River site (F. Syms, personal communication; and M. Gribb, personal communication), as documented in Fig. 6. These materials are silts and sands, and soundings were correlated with permeability tests on samples recovered from adjacent boreholes. The permeability profiles are predicted from B_q–Q_t, F_r–Q_t, and B_q–F_r data, and shown in Fig. 7. These results for F_r–Q_t and B_q–F_r are evaluated for a friction angle of 30° and null cohesion, although evaluating for $\phi=10°$ overprints these data directly. Tip measured excess pore pressures are predominantly positive, representing contractile strains in the tip-local process zone. All soundings were completed at a standard penetration rate of 2 cm/s.

Measured permeabilities are on the order of 10^{-4} m/s and are recovered from laboratory permeameter tests on small samples. No in situ permeability data are available. Estimates of field scale permeability magnitudes for the silty sands are recovered from the grain-size distributions available for the site, and utilizing available correlations (Robertson 1990; Hryciw et al. 2003). These estimated magnitudes of permeability are uniformly higher than laboratory values, are not well constrained, but provide an important reference for the laboratory measured magnitudes. Field and laboratory estimates of permeability vary over only 1
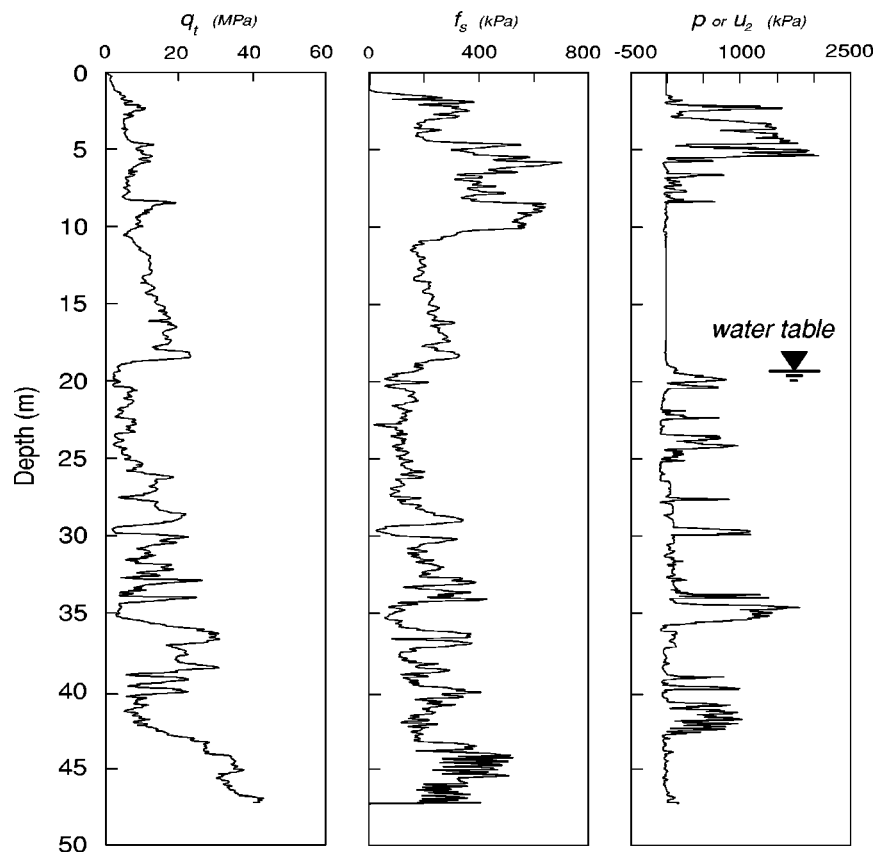
Fig. 6. Profile data from Savannah River site, defined by corrected tip resistance q_t, inclusive of corrected tip resistance q_t, sleeve friction f_s, and total pore pressure measured at cone shoulder u_2, or p in this analysis
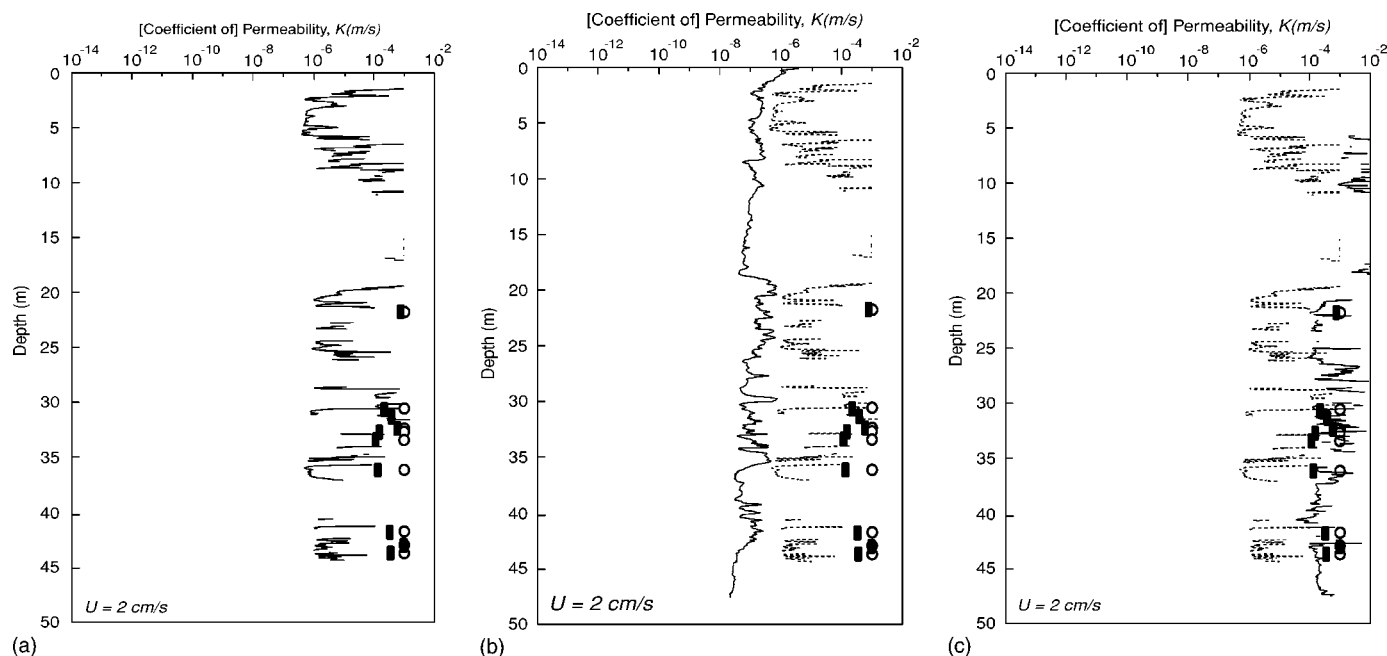

Fig. 7. Plots of predicted permeability with depth at Savannah River site. Permeability profiles are determined from data pairs: (a) $B_q - Q_t$ [Eq. (9)], (b) $F_r - Q_t$ [Eq. (10)], and (c) $B_q - F_r$ [Eq. (11)] to recover magnitudes of K_D for assumed $\phi = 30°$ (solid). Results for $\phi = 10°$ are indistinguishable from that for $\phi = 30°$ in (b) and (c) (not shown). Dotted lines in (b) and (c) represent permeability determined for friction angles determined with depth from Eq. (6) and used in Eq. (10) [panel (b)] and Eq. (11) [panel (c)], respectively. Squares and circles represent measured permeabilities from both laboratory permeameter tests and grain size distribution tests, respectively.
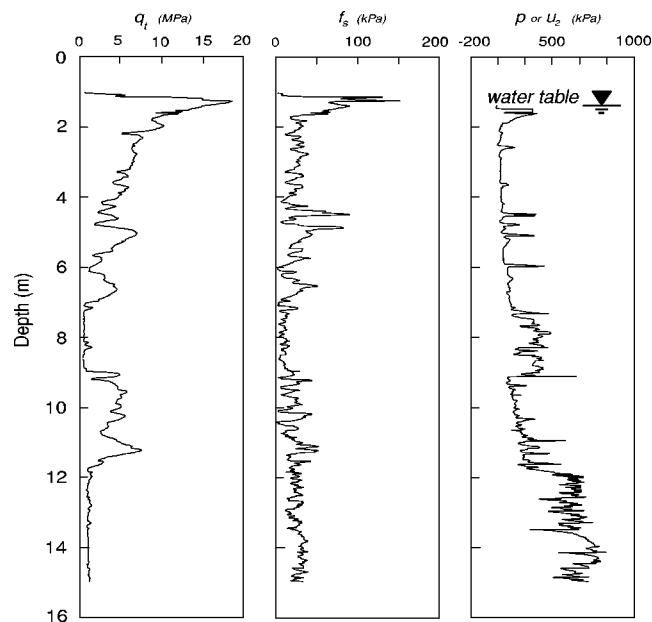
Fig. 8. Profile data from Treasure Island test site, CPTU01, defined by corrected tip resistance q_t, sleeve friction f_s, and total pore pressure measured at cone shoulder u_2, or p in this analysis

order of magnitude. The predictions recovered from magnitudes of $B_q - Q_t$ [Eq. (9)] and $B_q - F_r$ [Eq. (11)] provide the closest evaluations of permeabilities, with the $B_q - Q_t$ results sampling the higher range of the distribution. The predictions recovered from magnitudes of $F_r - Q_t$ [Eq. (10)] provide the poorest correlations. If the frictional strength is evaluated with depth from Eq. (6), with

$c_R = 0$, and then used to evaluate K_D from Eqs. (10) and (11), the dotted curves of Figs. 7(b and c) result. These dotted curves are identical to the sounding profile for $K_D = 1/B_q Q_t$ of Fig. 7(a). This results from Eqs. (10) and (11) represent only a single equation, $K_D = 1/B_q Q_t$, if consistent magnitudes of ϕ are used.

Treasure Island Test Site

Raw data are available for CPT soundings at the Treasure Island test site, in San Francisco, Calif. (Richard and Alba 2000) and are reported in Fig. 8. The site comprises a layered deposit of sand hydraulic fill. The full suite of CPT indices are available, inclusive of measured tip resistance q_t, sleeve friction f_s, and shoulder-measured pore pressure u_2 (or p), enabling magnitudes of nondimensional permeability K_D to be recovered. Magnitudes of nondimensional permeability K_D are converted to permeability magnitudes, directly, and plotted with depth in Fig. 9, similar to those for the Savannah River in Fig. 7. Permeability estimates, from grain size distributions (silty sands), determined for samples recovered from adjacent boreholes, are in the range $10^{-4} - 10^{-5}$ m/s. Estimates of permeability using the ensemble suite of metrics, $B_q - Q_t$, $F_r - Q_t$, and $B_q - F_r$, are on the order of $10^{-3} - 10^{-7}$ m/s, where frictional strength is arbitrarily set at $\phi = 30°$. The pore pressure data provide the closest evaluation of permeabilities, apparent in the sounding using $B_q - Q_t$. The consistency between estimates recovered independently from $B_q - Q_t$ [Eq. (9)] and $B_q - F_r$ data is taken as reasonable predictions of the permeability. In this case also, estimates from $F_r - Q_t$ provide the poorest estimate. For estimates using $B_q - F_r$ data, measured induced pore pressure magnitudes are small. Correspondingly, absent on the profile for $B_q - F_r$ are inadmissible predictions of permeability, that yield negative magnitudes. The use of the $F_r - Q_t$ [Eq. (10)] data produces permeabilities that are consistently lower
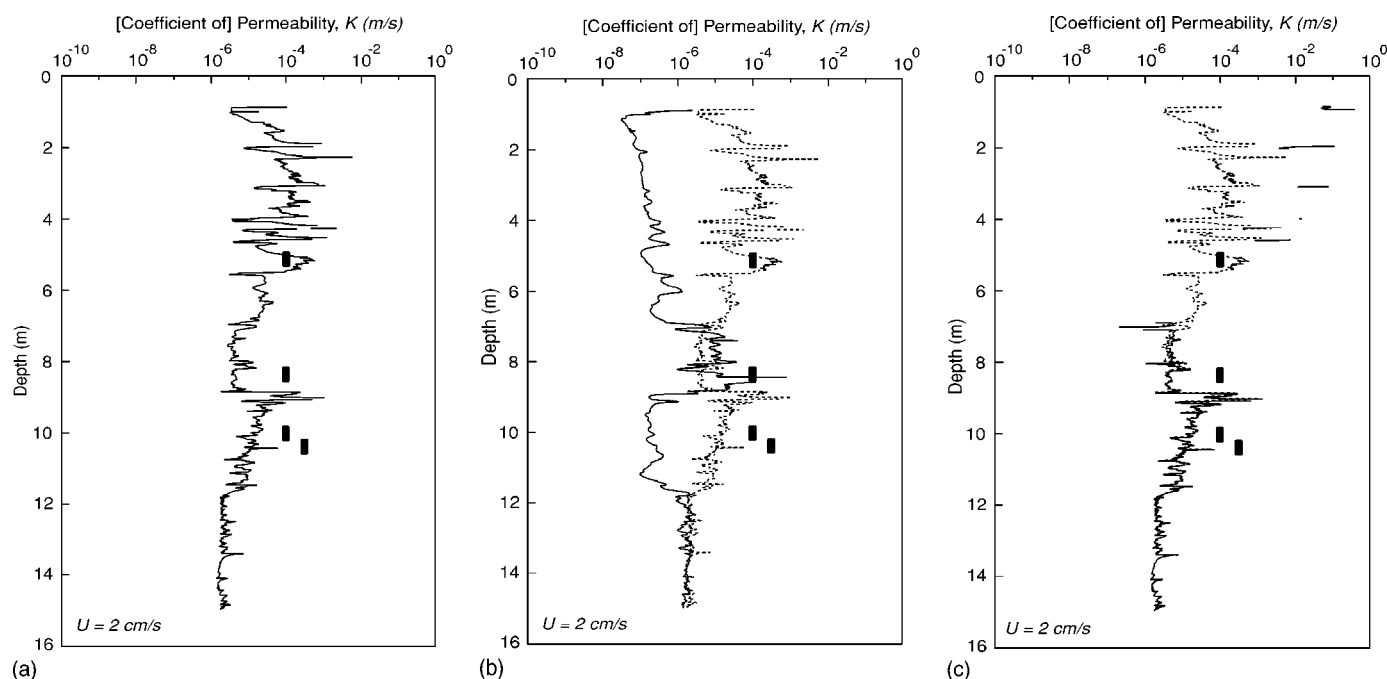

Fig. 9. Plots of predicted permeability with depth at Treasure Island test site CPTU01. Permeability profiles are determined from data pairs: (a) $B_q - Q_t$ [Eq. (9)], (b) $F_r - Q_t$ [Eq. (10)], and (c) $B_q - F_r$ [Eq. (11)] to recover magnitudes of K_D for assumed $\phi = 30°$ (solid). Results for $\phi = 10°$ are indistinguishable from that for $\phi = 30°$ in (b) and (c) (not shown). Dotted lines in (b) and (c) represent permeability determined for friction angles determined with depth from Eq. (6) and used in Eq. (10) [panel (b)] and Eq. (11) [panel (c)], respectively. Filled squares represent permeabilities estimated from measured grain size distribution
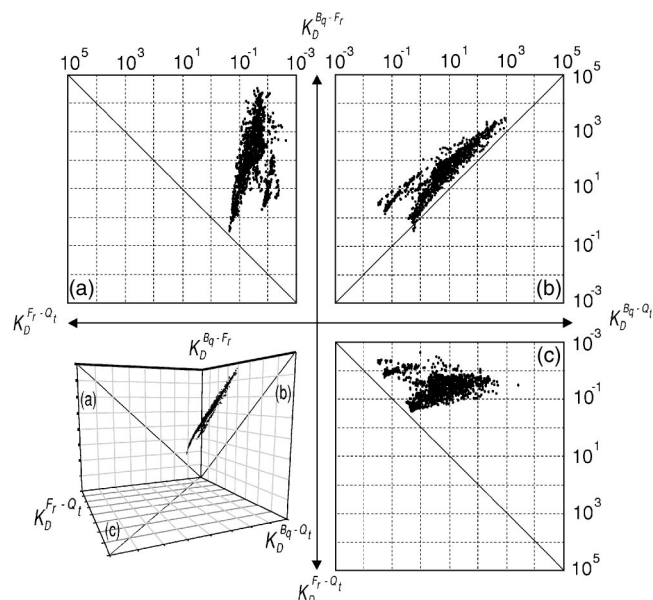
Fig. 10. Plots of K_D evaluated from three independent methods, for Savannah River site data. $K_D^{B_q-F_r}$ is evaluated from Eq. (11), $K_D^{B_q-Q_t}$ is evaluated from Eq. (9), and $K_D^{F_r-Q_t}$ is evaluated from Eq. (10) ($\phi=30°$).
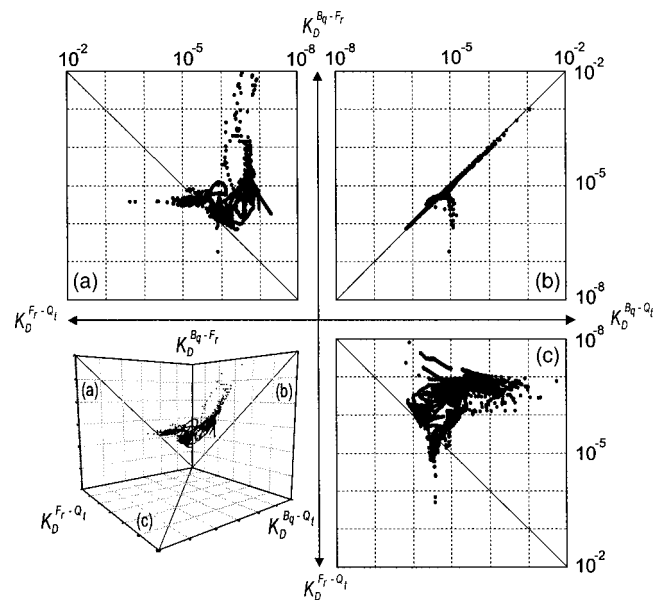

Fig. 11. Plots of K_D evaluated from three independent methods, for Treasure Island test site. $K_D^{B_q-F_r}$ is evaluated from Eq. (11), $K_D^{B_q-Q_t}$ is evaluated from Eq. (9), and $K_D^{F_r-Q_t}$ is evaluated from Eq. (10) ($\phi=30°$).

than magnitudes recovered from the grain size distribution tests and are furthest from the estimated magnitude. Again, where frictional strength (ϕ) is determined with sounding depth through Eq. (6), the predictions from all methods are identical, reflecting $K_D=1/B_qQ_t$, as shown in the dotted curves of Figs. 7(b and c).

Independent Evaluations of K_D

Only sparing permeability data are available to correlate with the evaluations of the previous. An alternative method of partially validating these evaluations is to compare the magnitudes of permeability predicted by each of the potential methods embodied in Eqs. (9), (10), and (11). Each of these relations allows the evaluation of an independent magnitude of the parameter K_D, that may be plotted in pairs, as illustrated in Fig. 10 for the Savannah River Site data, and in Fig. 11 for the Treasure Island test site data. In the absence of independently measured permeability data, the measure of how close cross plots of Eqs. (9), (10), and (11) plot to the leading diagonal, gives a sense of how useful the parameters may be in evaluating K_D, and hence, K. Specifically this gives a picture of how consistent the individual evaluations may be in determining permeability, K.

The cloud of ensemble data points, recovered for the Savannah River site are shown in Fig. 10. As previously conjectured, the plots of Figs. 7(a and b), representing plots of B_q-Q_t and B_q-F_r, respectively, are likely the most useful in yielding reliable predictions of permeability. Fig. 10 examines only the internal consistency in using cone metrics to predict K_D. Of all the outcomes, Fig. 10(b) most closely demonstrates consistency between metric pairs, where the data should plot on the leading diagonal if K_D magnitudes evaluated from each of these index pairs were identical. As apparent in the figure, this is not precisely the case, but there is some structure to the plot, with all data distributed above this diagonal. Significantly, Fig. 10(b) suggests consistency between the pairs B_q-F_r and B_q-Q_t; where each pair includes the magnitude of the pore pressure parameter, B_q, directly. This result

is independent of the previous analysis of data that also suggest that the two data pairs of B_q-Q_t and B_q-F_r are most useful in reducing sounding records for permeability data. The lack of structure apparent in Figs 10(a and c) is taken as inconclusive, but suggest that pairs that include the magnitude of pore pressure parameter, B_q, directly, perform the best. Where a similar exercise is completed for the Treasure Island data, and reported in Fig. 11, a similar conclusion may be drawn—that those indices incorporating measured pore pressures provide the most robust method of determining permeability magnitudes. Where permeabilities are derived from cone-metric-derived frictional strengths (dotted lines in Figs. 7 and 9), the data plot directly on the diagonals of Figs. 10 and 11. This is because predictions using only Eqs. (9), (10), and (11), reduce simply to $K_D=1/B_qQ_t$, where consistent frictional strengths are incorporated.

Conclusions

Solutions are developed for the pore pressure fields that develop around infinitesimal-radius and finite-radius penetrometers inserted under steady-state flow conditions. The maximum pore pressure, recorded at the penetrometer tip is, suggested as indicative of the permeability of the surrounding soil, since the ability for fluids to dissipate is conditioned by this primary index of peak pressure. For either the infinitesimal-radius or the finite-radius penetrometer, the response is governed by the unified nondimensional parameter $K_D=4K\sigma'_{v0}/Ua\gamma_w$. This parameter balances the agents that develop large pressures, present in the denominator, with those that result in their dissipation, present in the numerator. This index is useful in recovering permeability magnitudes from on-the-fly penetration. Solutions are developed for the pore pressure field that develops around an infinitesimal-radius penetrometer, assuming elastic behavior, and around a finite-radius penetrometer, accommodating a nondilatant process zone.

These solutions enable normalized cone penetration metrics of

pore pressure ratio B_q, sleeve friction F_r, and tip resistance Q_t to be related directly to a nondimensional permeability K_D, and thereby to provide estimates of permeability. Most significant is the ability to contour plots of B_q-Q_t and F_r-Q_t for magnitudes of K_D, and hence for permeability. Furthermore, these relations may be used to define permeability distributions with sounding depth, as a site investigation tool. Importantly, existing cone metrics may be used to determine permeability magnitudes, without modification, provided the limits of applicability of the method are recognized. The method is applicable, depending on the magnitudes of the component parameters of K_D, only for "intermediate" magnitudes of permeability; these are in the approximate range $10^{-4}-10^{-7}$ m/s. At higher permeabilities than these, the penetration process is drained, and all excess pore pressures dissipate as quickly as they are developed. At lower permeabilities than these, the behavior is undrained, the system is not a steady flow regime, and pressures are related to the tip-local stresses developed during penetration, only. Thus, only permeabilities within this approximate intermediate range may feasibly be determined from the penetration process, for standard penetration at 2 cm/s. This range may be extended by varying insertion rates or penetrometer radius.

When applied to well constrained data from two sites, the reduction methods are shown to be capable of recovering the magnitudes of permeability. For the cases evaluated here, the use of the independent data pair B_q-Q_t yields the closest and most consistent evaluations of permeability. In the two studies, the pair B_q-F_r also yields acceptable correlations. The pair F_r-Q_t give the poorest results. Prediction from these parameters is less robust. Where frictional strength is determined with depth from the sounding data, then predictions of permeabilities from all three data pairs reduce to $K_D=1/B_qQ_t$.

Acknowledgments

Notation

The following symbols are used in this paper:

A_c = projected frontal area of the cone [L²];
A_n = cross-sectional area of load cell or shaft [L²];
a = penetrometer radius [L];
a_n = area ratio of the cone (A_n/A_c);
B_q = dimensionless pore pressure ratio $(p-p_s)/(q_t-\sigma_{v0})$;
c = cohesion;
c_R = dimensionless cohesion $c/(q_t-\sigma_{v0})$;
c_v = coefficient of consolidation [L²T⁻¹];
dV = volume change per unit time in tip process zone [L³T⁻¹];
F_r = dimensionless friction factor $f_s/(q_t-\sigma_{v0})$;
f_s = magnitude of sleeve friction [FL⁻²];
K = (coefficient of) permeability [LT⁻¹];
K_D = dimensionless permeability $(4K\sigma'_{v0})/(Ua\gamma_w)$;
$K_D^{B_q-F_r}$ = dimensionless (coefficient of) permeability determined from B_q-F_r data;

$K_D^{B_q-Q_t}$ = dimensionless (coefficient of) permeability determined from B_q-Q_t data;
$K_D^{F_r-Q_t}$ = dimensionless (coefficient of) permeability determined from F_r-Q_t data;
p = absolute pore fluid pressure (u_2) (FL⁻²);
p_s = initial static fluid pressure (FL⁻²);
$p-p_s$ = excess pore pressure (FL⁻²);
Q_t = dimensionless tip resistance $(q_t-\sigma_{v0})/\sigma'_{v0}$;
q_c = measured tip resistance (FL⁻²);
q_t = corrected tip resistance $q_c+(1-a_n)(p-p_s)$ (FL⁻²);
r_h = radius of hydraulic zone [L];
r_m = radius of mechanical tip process zone [L];
U = penetrometer penetration rate [LT⁻¹];
x = location of pressure transducer behind tip [L];
γ_w = unit weight of water [FL⁻³];
$\sigma_{h0}, \sigma'_{h0}$ = initial horizontal stress and effective stress [FL⁻²];
$\sigma_{v0}, \sigma'_{v0}$ = initial vertical stress and effective stress [FL⁻²]; and
ϕ = soil friction angle.

References

Auxt, J. A., and Wright, D. (1995). "Environmental site characterization in the United States using the cone penetrometer." *Proc., CPT'95*, Linkoping, Sweden, 387–392.

Baligh, M. M. (1985). "Strain path method." *J. Geotech. Eng.*, 111(9), 1108–1136.

Baligh, M. M., and Levadoux, J. N. (1986). "Consolidation after undrained piezocone penetration. II: Interpretation." *J. Geotech. Eng.*, 112(7), 727–745.

Burns, S. E., and Mayne, P. W. (1998). "Monotonic and dilatory pressure decay during piezocone tests in clay." *Can. Geotech. J.*, 35(6), 1063–1073.

Campanella, R. G., and Robertson, P. K. (1988). "Current status of the piezocone test." *Penetration testing 1988*, J. de Ruiter, ed., ISOPT-1, A.A. Balkema, Rotterdam, The Netherlands, 93–116.

Chiang, C. Y., Loos, K. R., and Klopp, R. A. (1992). "Field determination of geological/chemical properties of an aquifer by cone penetrometry and head-space analysis." *Ground Water*, 30(3), 428–436.

Cividini, A., and Gioda, G. (1988). "A simplified analysis of pile penetration." *Proc., 6th Int. Conf. Numerical Methods Geomechanics*, 1043–1049.

Danziger, F. A. B., Almeida, M. S. S., and Sills, G. C. (1997). "The significance of the strain path analysis in the interpretation of piezocone dissipation data." *Geotechnique*, 47(5), 901–914.

Douglas, B. J., and Olsen, R. S. (1981). Soil classification using electric cone penetrometer. Cone penetration testing and experience. *Proc. ASCE National Convention*, ASCE, New York, 209–227.

Elsworth, D. (1990). "Theory of partially drained piezometer insertion." *J. Geotech. Eng.*, 116(6), 899–914.

Elsworth, D. (1991). "Dislocation analysis of penetration in saturated porous media." *J. Eng. Mech.*, 117(2), 391–408.

Elsworth, D. (1992). "Pore pressure response due to penetration through layered media." *Int. J. Numer. Analyt. Meth. Geomech.*, 16(1), 45–64.

Elsworth, D. (1993). "Analysis of piezocone data using dislocation based methods." *J. Geotech. Eng.*, 119(10), 1601–1623.

Elsworth, D. (1998). "Indentation of a sharp penetrometer in a poroelastic medium." *Int. J. Solids Struct.*, 35(34–35), 4895–4904.

Gribb, M. M., Simunek, J., and Leonard, M. F. (1998). "Development of cone penetrometer method to determine soil hydraulic properties." *J. Geotech. Geoenviron. Eng.*, 124(9), 820–829.

House, A. R., Olivera, J. R. M. S., and Randolph, M. F. (2001). "Evaluating the coefficient of consolidation using penetration tests." *Int. J. Phys. Model.*, 1(3), 19–27.

Hryciw, R. D., Shin, S., and Ghalib, A. M. (2003). "High resolution site

characterization by visCPT with application to hydrogeology." *Proc., 12th Panamerican Conf. on Soil Mechs.*, Boston, 293–298.

Kegley, W. P. (1993). "Distribution of permeability at the MWD well field, Savannah River Site, South Carolina." Masters thesis, Clemson Univ., Clemson, S.C.

Kiousis, P. D., and Voyiadjis, G. Z. (1985). "Lagrangian continuum theory for saturated porous media." *J. Eng. Mech.* 111(10), 1277–1288.

Konrad, J. M., and Frechette, P. (1995). "The piezocone-permeameter probe: A promising tool." *Proc., Geoenvironmental 2000, Charact., Contain., Remed., and Perform. Environmental Geotechnics, GSP No. 48*, Vol. 1, 123–137.

Kurup, P. U., Voyiadjis, G. Z., and Tumay, M. T. (1994). "Calibration chamber studies of piezocone tests in cohesive soils." *J. Geotech. Eng.*, 120(1), 81–107.

Levadoux, J. N., and Baligh, M. M. (1986). "Consolidation after undrained piezocone penetration. I: Prediction." *J. Geotech. Eng.*, 112(7), 707–726.

Lowry, B. (1998). "Cone permeameter in-situ permeability measurements with direct push techniques." *Rep. No. SEASF-MR-98-200*, Science and Engineering Associates, Inc.

Lunne, T., Robertson, P. K., and Powell, J. J. M. (1997). *Cone penetration testing in geotechnical practice*, Blackie Academic.

Manassero, M. (1994). "Hydraulic conductivity assessment of slurry wall using piezocone test." *J. Geotech. Eng.*, 120(10), 1725–1746.

Mitchell, J. K., and Brandon, T. L. (1998). "Analysis and use of CPT in earthquake and environmental engineering." *Geotechnical site characterization*, Robertson and Mayne, eds., Vol. 1, Balkema, Rotterdam, The Netherlands, 69–96.

Olsen, R. S. (1994). "Normalization and prediction of geotechnical properties using the cone penetrometer test." *Technical Rep. No. GL-94-29*, U.S. Army Corps of Engineers, WES, Vicksburg, Miss., 322–322.

R, F., J. and Alba, P. (2000). "National geotechnical experimentation site at Treasure Island, California." *National Geotechnical Experimentation Sites.* ⟨http://www.unh.edu.nges⟩ 52–71.

Robertson, P. K. (1990). "Soil classification using the cone penetration test." *Can. Geotech. J.*, 27(1), 151–158.

Robertson, P. K., Campanella, R. G., Gillespie, D., and Greig, J. (1986). "Use of piezometer cone data." *Proc. Use of In Sit Tests in Geotechnical Engineering*, ASCE, New York, 1263–1280.

Robertson, P. K., Sully, J. P., Woeller, D. J., Lunne, T., Powell, J. J. M., and Gillespie, D. G. (1992). "Estimating coefficient of consolidation from piezocone tests." *Can. Geotech. J.*, 29(4), 539–550.

Scaturo, D. M., and Wissowson, M. A. (1997). "Experimental evaluation of a drive-point ground-water sampler for hydraulic conductivity measurement." *Ground Water*, 35(4), 713–720.

Schmertmann, J. H. (1978). "Guidelines for cone penetration test: Performance and design." *Technical Rep. FHWA-TS-78-209*, FHWA, Washington, D.C.

Smythe, J. M., Bedient, P. B., Klopp, R. A., and Chiang, C. Y. (1989). "An advanced technology for the in situ measurement of heterogeneous aquifers." *Proc., Conf. New Field Tech. Quant. Phys. Chem. Prop. Heter. Aquifers*, 605–628.

Song, C. R., Voyiadjis, G. Z., and Tumay, M. T. (1999). "Determination of permeability of soils using the multiple piezo-element penetrometer." *Int. J. Numer. Analyt. Meth. Geomech.*, 23(13), 1609–1629.

Teh, C., and Houlsby, G. (1991). "An analytical study of the cone penetration test in clay." *Geotechnique*, 41, 17–34.

Thibault, J. J. (1996). "Numerical model of the McQuenn Branch-Mill Creek divide, Savannah River site, South Carolina; Characterization of groundwater flow in tertiary sand aquifers." Masters thesis, Clemson Univ., Clemson, S.C.

Torstensson, B. A. (1977). "The pore pressure probe." *Nordiske Geotekniske Mote*, 34(34), 1–34.15.

van den Berg, P. (1994). "Analysis of soil penetration." PhD thesis, Delft Univ., Delft, The Netherlands.

Voyiadjis, G. Z., and Abu-Farsakh, M. Y. (1997). "Coupled theory of mixtures for clayey soils." *Comput. Geotech.*, 20(3/4), 195–222.

Voyiadjis, G. Z., and Song, C. R. (2000). "Finite strain ansiotropic Cam Clay model with plastic spin. II: Application to piezocone test." *J. Eng. Mech.* 126(10), 1020–1026.

JOURNAL OF GEOTECHNICAL AND GEOENVIRONMENTAL ENGINEERING © ASCE / MAY 2005 / **653**

J. Geotech. Geoenviron. Eng., 2005, 131(5): 643-653